JOURNAL OF OPTOELECTRONICS AND ADVANCED MATERIALS, Vol. 11, No. 12, December 2009, p. 1891 - 1898

Combined method of spectroscopic ellipsometry and photometry as an efficient tool for the optical characterisation of chalcogenide thin films

D. FRANTA, D. NEČAS, I. OHLÍDAL*, M. HRDLIČKA[a], M. PAVLIŠTA[a], M. FRUMAR[a], M. OHLÍDAL[b]
Department of Physical Electronics, Faculty of Science, Masaryk University, Kotl´aˇrsk´a 2, 611 37 Brno, Czech Republic
[a]Department of General and Inorganic Chemistry, University of Pardubice, n´am. ˇCs. Legi´ı 565, 53210 Pardubice, Czech Republic
[b]Institute of Physical Engineering, Faculty of Mechanical Engineering, Brno University of Technology, Technick´a 2, 61669 Brno, Czech Republic

The optical characterisation of the $As_{33}Se_{67}$ and $Ge_2Sb_2Te_5$ chalcogenide thin films is carried out using the combined method of VASE and SR. This method permits to determine both structural and dispersion parameters describing the thin films exhibiting various defects. The structural model is based on including roughness, overlayers and thickness non-uniformity. The dispersion models are based on parametrisation of the joint density of states. These models, unlike the classical models derived from the Lorentz oscillator model, can describe finite bands which allows to introduce a parameter proportional to the density of electrons. It is shown that this method enables to investigate quantitatively changes in the electronic structure of the materials caused by phase transitions which is demonstrated on the $Ge_2Sb_2Te_5$. It is shown that the combined method with including true structural and dispersion models is a powerful tool for the optical characterisation of thin films exhibiting disordered structure.

(Received July 5, 2009; accepted November 12, 2009)

*Keywords:*Ellipsometry, Photometry, Chalcogenige, Thin film

1. Introduction

Chalcogenide thin films are very useful for practical applications. They are employed, for example, as inorganic resists, media for recording in holography, materials for optoelectronics, etc. Their optical properties are significant for the applications mentioned. Moreover, the optical properties films provide detailed information about electronic structure of the film material and its changes. Therefore, a considerable attention has been devoted to optical characterisation of various chalcogenides films[1-13].

In many studies, the optical characterisation of the chalcogenide thin films is connected with determining the optical constant in the transparency region of the films with the aim of evaluating the Tauc gap [1, 7, 10, 11]. However, such approach based on determination of this only one parameter does not yield complete information concerning the optical properties and the electronic structure of materials forming these films and, moreover, it does not take into account the Kramers–Kronig consistency of dielectric response. The approach based on determination of the Tauc band gap mostly employs the measurement of the spectral transmittance [7, 10] or combination of spectral transmittance and reflectometry [1, 8]. The disadvantage of this approach consist in necessity of using relatively thick chalcogenide films and non-absorbing transparent substrates. Of course, if the substrates are absorbing in principle it is possible to use the measurement of the spectral reflectance of the chalcogenide films, i. e. spectroscopic reflectometry (SR), for determining the Tauc gap. In this case it is necessary to use a suitable dispersion model of the optical constants of the chalcogenide films [3]. However, in practise this approach often fails because of the various defects such as boundary roughness, overlayers and thickness non-uniformity occurring in the films characterised. Better results of the optical characterisation of the films with defects can be achieved by using variable angle spectroscopic ellipsometry (VASE) [2, 8, 9]. To our experience the most efficient method for characterising thin films with defects is the method based on combination of VASE and SR applied at near-normal incidence [4, 5, 12] or normal spectroscopic transmittance [6]. Within this combined method the simultaneous interpretation of the ellipsometric and reflectometric data is performed by means of corresponding structural and dispersion models of the films.

In this paper the combined optical method will be used to perform the complete optical characterisation of $As_{33}Se_{67}$ and $Ge_2Sb_2Te_5$ (GST) films deposited on silicon single crystal substrates. It will be shown that using this method one can determine the thickness values, optical constants and parameters describing boundary roughness, thickness non-uniformity and overlayer of the films studied. The spectral dependencies of the optical

constants will be determined using the dispersion model based on parametrisation of the joint density of electronic states (PJDOS) and, therefore, the material parameters determining electronic structure of films will be be evaluated. Thus, in this paper it will be shown that the combined method of VASE and SR is very useful method for the complete optical characterisation of the various chalcogenide thin films.

2. Data processing

Within the combined method of VASE and SR, the spectral dependencies of the ellipsometric quantities measured for several angle of incidence within the interval 55^{O}–75^{O} were fitted simultaneously with the spectral dependence of reflectance measured at near-normal incidence for each sample under investigation. The spectral dependencies of the ellipsometric quantities were measured using phase modulated Jobin Yvon UVISEL ellipsometer within spectral region 0.6–6.5 eV. The spectral dependencies of reflectance were measured by Perkin Elmer Lambda 45 spectrophotometer with reflectance accessory for the incidence angle of 6^{O} within the spectral region 1.24–6.5 eV. For the data fitting the following merit function *S* was used:

$$S = \sum_{\lambda_i \theta_{0,i}} \left| (I(\lambda_i, \theta_{0,i}) - I_i^{\exp} \right|^2 w_i + \sum_{\lambda_j} [(R(\lambda_j) - R_j^{\exp}]^2 w_j \qquad (1)$$

where *i* and *j* number individual data points; λ and θ_0 are the wavelength and the angle of incidence, respectively; **I** is the vector representing the associated ellipsometric parameters; *R* denotes the reflectance; *w* are the weights of measured quantities determined using the estimated experimental accuracy; superscript *exp* denotes experimental values of the individual quantities. Note that the reflectance *R* is the M_{00} component of the Mueller matrix and the associated ellipsometric parameters *Is*, $I_{c,II}$ and $I_{c,III}$, forming vector **I**, are equal to the independent components of the corresponding normalised Mueller matrix of isotropic system. Hence, it is advantageous to combine the processing of the associated ellipsometric parameter and reflectance because these quantities give a complete information on the light beam reflected from the sample studied.

The theoretical values of the measured quantities were calculated on the basis of the structural and dispersion models constructed for the individual chalcogenide thin films under study.

3. Structural model

It was assumed that the films were isotropic and homogeneous. Furthermore, it was assumed that a very thin rough overlayer was present on the upper boundaries of the film. This rough overlayer was represented by the identical thin film. The influence of the roughness was included into the formulae for the optical quantities by means of the Rayleigh–Rice Theory (RRT) [14-18]. It should be noted that on the upper boundaries of the overlayers a macroscopic dust particles occurred. These particles evidently scattered incident light. The influence of the dust particles was included into the formulae using a constant attenuation factor without dispersion having the effect only on the reflectance. For some sample the existence of the thickness non-uniformity was taken into account at calculating the optical quantities. The influence of the thickness non-uniformity was considered using the following formula for the Mueller matrix representing system ⟨**M**⟩:

$$\langle \mathrm{M} \rangle = \int M(h) w(h) dh \qquad (2)$$

where *h* is the local thickness and *w*(*h*) is thickness distribution density [19]. The Mueller matrix **M**(*h*) was calculated using the 2×2 matrix formalism [20] allowing to express the coherent local field inside the film system.

4. Dispersion models

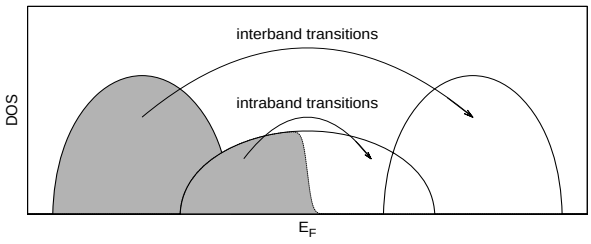

Fig. 1. Schematic diagram of interband and intraband electronic transitions. Shaded area depicts occupied electronic states according to the Fermi–Dirac statistics. Symbol EF denotes the Fermi energy.

The imaginary part of dielectric function *i*(*E*) of disordered materials is expressed by the following formula based on the Fermi golden rule [21-25]:

$$\varepsilon_i(E) = \left(\frac{eH}{mE}\right)^2 \frac{1}{4\pi B_o \varepsilon_o} \sum_{j,k} \left| p_{j \to k} \right|^2 [\Im_{j \to k}(E) - \Im_{j \leftarrow k}(E)] \qquad (3)$$

where *e*, *h*, *m*, ε_0 and B_0 are electron charge, Planck's constant, electron mass, permittivity of vacuum and certain part of Brillouin zone of corresponding crystalline material, respectively. The function $\Im_{j \to k}(E)$ represents the absorption of photon with energy *E* which excites the electron from *j*-th band to *k*-th band, i. e. from occupied state with energy *S* to empty state with energy *S*+*E*. The function $\Im_{jk}(E)$ represent the reverse process (stimulated

emission). The magnitudes of the matrix elements $|p_{j\to k}|$ and $|p_{jk}|$ expressing the probabilities of both process are equal, i. e. $|p_{j\to k}|=|p_{jk}|$, and they are assumed to be constant for all transitions from *j*-th to *k*-th band. The summation in Eq. (3) is performed over all possible transitions. Terms with $j\neq k$ correspond to interband transitions while terms with $j=k$ correspond to intraband transitions (see Fig. 1). The function $\mathcal{J}_{j\to k}(E)$ is analogous to joint density of states (JDOS) function introduced for crystalline materials [24] and can be expressed as follows:

$$\mathfrak{I}_{j\to k}(E)=\int_{-\infty}^{\infty} f_e N_j(S)\, f_h(S+E) N_k(S+E)\,dS \quad (4)$$

where the functions $\mathcal{N}_j$ and $\mathcal{N}_k$ are the densities of states (DOS) of electrons in the initial and the final bands. The electron energy changes from *S* to *S*+*E* during the process. The functions *fe* and *fh* denote the probability of occupation of electron and hole states given by the Fermi–Dirac distribution:

$$f_e(S)=\frac{1}{\exp[(S-E_F)/k_BT]+1}=1-f_h(S) \quad (5)$$

Note that the function $\mathcal{J}_{jk}(E)$ for $E<0$ ensures the antisymmetry of dielectric response and fulfils the following relations:

$$\mathfrak{I}_{j\leftarrow k}(E)=\mathfrak{I}_{j\to k}(-E) \quad \text{and} \quad \mathfrak{I}_{j\leftarrow k}(E)\neq\mathfrak{I}_{k\to j}(E) \quad (6)$$

Formula (3) can be simplified by incorporating the multiplicative factors, including momentum matrix elements, into the JDOS, obtaining the following formula

$$\varepsilon_i(E)=\frac{1}{E^2}\sum_{j,k} C_{jk} J_{jk}(E) \quad (7)$$

where factors C_{jk} represent different probabilities of individual transitions. However, usually most of them can be put equal to unity or zero. Each function J_{jk} in Eq. (7) describes both processes, i. e. absorption and emission, and it is called unnormalized JDOS:

$$J_{jk}(E)=J_{j\to k}(E)-J_{j\to k}(E)=J_{j\leftarrow k}(-E) \quad (8)$$

where the absorption term $J_{j\to k}(E)$ is expressed by formula analogous to (4)

$$\mathrm{J}_{j\to k}(E)=\int_{-\infty}^{\infty} f_e(S) N_j(S)\, f_h(S+E) N_k(S+E)\,dS \quad (9)$$

here functions *N* are the unnormalized DOS and they differ from $\mathcal{N}$ only by multiplicative factors. The function *N* and *J* are called unnormalized as they are not normalised to the total density of states (for details see [25]).

The Eqs. (7)–(9) form the basis of the parametrised density of states (PDOS) and parametrised joint density of states (PJDOS) models [26]. In order to obtain the complete dielectric function these equations have to be complemented by Kramers–Kronig integral expressing the real part of dielectric function [27]:

$$\varepsilon_r(E)=1+\frac{2}{\pi}\int_0^{\infty}\frac{X\varepsilon_i(X)}{X^2-E^2}dX \quad (10)$$

In this paper we will only perform parametrisation of the JDOS, i. e. we will use the PJDOS models.

We will employ two PJDOS models for expressing the interband transitions. The first of them is the already published three parameter PJDOS (PJDOS3) model [13, 25, 26] and the second corresponds to the new six parameter PJDOS (PJDOS3) model. For expressing the intraband transitions we will utilise recently published two parameter PJDOS (PJDOS2) model [13].

4.1 PJDOS3 model of interband transitions

Within this model the JDOS function representing transitions from the fully occupied *j*-th band to empty *k*-th band is expressed as follows:

$$J_{j\to k}(E)=\begin{cases}\dfrac{30Q^2(E-E_g)^2(E-E_h)^2}{0} & \text{for } E_g<E<E_h\\ \text{otherwise} & \end{cases} \quad (11)$$

where Q^2, *Eg* and *Eh* are total joint density of states of the transitions, minimum energy of transitions (band gap) and maximum energy of transitions, respectively. The constant factors in Eq. (14) are chosen so that parameters Q_j and Q_k are proportional to the numbers of states in the *j*-th and *k*-th band, respectively:

$$\int_0^{\infty} J_{jk}(E)\,dE=C_{jk}Q_jQ_k=Q^2 \quad (12)$$

The real and imaginary part of this contribution is calculated analytically from Eqs. (7), (8) and (10)

$$\varepsilon_{r,jk}(E)=\frac{60Q^2}{\pi(E_h-E_g)^5}\left[b\ln\left|\frac{E+E_h}{E+E_g}\right|+c\ln\left|\frac{E-E_h}{E-E_g}\right|-d\right] \quad (13)$$

$$\varepsilon_{i,jk}(E)=\frac{J_{jk}(E)}{E^2} \tag{14}$$

where

$$b=\frac{y+x}{2E^2},\quad c=\frac{y-x}{2E^2},\quad d=\frac{E_g^2E_h^2}{E^2}\ln\left|\frac{E_h}{E_g}\right|+\frac{3(E_h^2-E_g^2)}{2}$$

$$x=2E[E_h(E_g^2+E^2)+E_g(E_h^2+E^2)]$$

$$y=E^2(E_h^2+E_g^2+4E_gE_h+E^2)+E_g^2E_h^2$$

Note that in points 0, *Eg* and *Eh* the function $\varepsilon_{r,jk}(E)$ must be represented by values of the limits in these points.

4.2 PJDOS6 model of interband transitions

Sometimes the three parameter PJDOS model is not sufficient for interpretation of experimental data. In this case it is necessary to modify the form of the JDOS function expressing the transition between two bands. We, therefore, extended the PJDOS3 model by introducing three new parameters enabling such modification. The first of them, *Ec*, determines the position of the maximum of the JDOS function (central energy of transitions). The second and third parameters *G* and *H* modify the form of JDOS function by adding third order terms within intervals (E_g, E_c) and (E_c, E_h), respectively. When $E_c=(E_g+E_h)/2$, $G=0$ and $H=0$ the six parameter model is identical with three parametric model. The real and imaginary parts of this contribution have the following analytical form:

$$\varepsilon_{r,jk}(E)=\frac{2}{\pi}[A_2^-F_2(E,E_g,E_c)-A_2^+F_2(E,E_h,E_c)-A_3^-F_3(E,E_g,E_c)+A_3^+F_3(E,E_h,E_c)] \tag{15}$$

$$\varepsilon_{i,jkl}(E)=A_2^-f_2(E,E_g,E_c)+A_2^+f_2(E,E_h,E_c)+A_3^-f_3(E,E_g,E_c)+A_3^+f_3(E,E_h,E_c) \tag{16}$$

where

$$A_2^-=\frac{Q^2}{N}\frac{1-G}{(E_c-E_g)^4},\quad A_2^+=\frac{Q^2}{N}\frac{1-H}{(E_h-E_c)^4}$$

$$A_3^-=\frac{Q^2}{N}\frac{G}{(E_c-E_g)^6},\quad A_3^+=\frac{Q^2}{N}\frac{H}{(E_h-E_c)^6}$$

$$f_n(E,E_1,E_2)=\frac{(E-E_1)^n(-E_3-E)^n}{E^2}\ for\left|E-\frac{(E_1+E_2)}{2}\right|\le\left|\frac{E_1-E_2}{2}\right|=0$$

otherwise

$$N=\frac{8}{15}(E_c-E_g)(1-\frac{G}{7})+\frac{8}{15}(E_h-E_c)(1-\frac{H}{7})$$

$$F_2(E,E_1,E_2)=\frac{E_2^2-E_1^2}{2}+a_2(E_2-E_1)+b_2\ln\frac{E_2}{E_1}+c_2^+\ln\left|\frac{E_2-E}{E_1-E}\right|+c_2^-\ln\frac{E_2+E}{E_1+E}$$

$$F_3(E,E_1,E_2)=\frac{E_2^4-E_1^4}{4}-2E_2(E_2^3-E_1^3)+l_3\frac{E_2^2-E_1^2}{2}+a_3(E_2-E_1)+b_3\ln\frac{E_2}{E_1}+c_3\ln\left|\frac{E_2-E}{E_1-E}\right|+d_3\ln\frac{E_2+E}{E_1+E}$$

$$E_3=E_1-2E_2\quad a_2=-4E^2\quad b_2=-\frac{E_1^2E_3^2}{E^2}$$

$$c_2^{\pm}=\frac{1}{2}(E_2^2-4E_1E_3+E_1^2+E_2-b_2)\pm\pm\frac{1}{2E}(a_2E^2+E_1^2E_3-E_1E_3^2)$$

$$a_3=E_3^3-9E_1E_3^2+9E_1^2E_3-E_1^3-6E_2E^2,\quad b_3=\frac{E_1^3E_3^3}{E^2}$$

$$c_3^{\pm}=\frac{1}{2}(-3E_1^3E_3-3E_1E_3^3+9E_1^2E_3^2+l_3E^2-b_3)\pm\pm\frac{1}{2E}(a_3E^2+3E_1^2E_3^3-3E_1^3E_3^2)$$

$$l_3=3E_3^2-9E_1E_3+3E_1^2+E^2$$

$$E_c=E_g+C(E_h-E_c)$$

From the foregoing it is seen that the following parameters must be found using the treatment of the experimental data in order to determine the spectral dependencies of the optical constants: $Q\in(0,\infty)$, $E_g\in(0,\infty)$, $E_h\in(E_g,\infty)$, $C\in(0,1)$, $G\in(-1,1)$ and $H\in(-1,1)$.

4.3 Intraband transitions

The contribution of intraband transitions can also be calculated using Eqs. (7)–(9). However, for *j*=*k* the unnormalized JDOS can be simplified as

$$J_{jj}(E)=\int_{-\infty}^{\infty}[f_e(S)-f_e(S+E)]N_j(S)N_j(S+E)dS \tag{17}$$

It can be shown that if the DOS changes slowly in vicinity of Fermi energy then for small energies the JDOS obtained from (17) is a linear function of energy:

$$J_{jj}(E) = N_j^2 E \tag{18}$$

Note that the Drude formula derived for free electrons exhibits the same linear dependence for small energies. Evidently the PJDOS3 model for interband transitions cannot be used if the Fermi energy lies inside the band even when the parameter *Eg* is put equal to zero because PJDOS3 is quadratic in vicinity of *Eg*. Therefore, it is necessary to find a new analytical model for describing intraband transitions. In our recent paper [13] we used the following parametrisation JDOS corresponding to the intraband transitions:

$$J_{jj}(E) \propto E(E_w - E)^2 (E + E_w)^2 \tag{19}$$

where *Ew* is the band width. The individual factors in Eq. (19) ensure the following properties: the first factor *E* linearity around zero, the second factor $(Ew\text{-}E)^2$ the quadratic form for energies in vicinity of *Ew* and third factor $(E+Ew)^2$ causes antisymmetry of JDOS. Similarly to the model of interband transitions the following two parametric analytical formula of dielectric response for intraband transitions can be derived:

$$\varepsilon_{i,j}(E) = \begin{cases} \dfrac{6{Q_j}^2 (E_w^2 - E)^2}{E_w^6 E} \text{.....} for: E < E_w \\ 0 \text{.....} otherwise \end{cases} \tag{20}$$

and

$$\varepsilon_{r,j}(E) = \frac{12 Q_j^2}{\pi E_w^6} \frac{(E_w^2 - E^2)^2}{2E} \ln\left|\frac{E_w - E}{E_w + E}\right| + E^2 E_w - \frac{5}{3} E_w^3 \tag{21}$$

5. Results and discussion

We applied the combined optical method for the optical characterisation of $As_{33}Se_{67}$ and $Ge_2Sb_2Te_5$ chalcogenide films. In this section the results corresponding to one selected sample of $As_{33}Se_{67}$ and selected sample $Ge_2Sb_2Te_5$ will be presented.

5.1 $As_{33}Se_{67}$

The bulk samples of composition $As_{33}Se_{67}$ were prepared from high purity (5N) elements by direct synthesis (800 ^{o}C, 24 hours) in evacuated quartz ampules using conventional melt quenching technique. Their thin films were prepared by classical thermal vacuum evaporation from finely powdered material evaporated from molybdenum boats. Deposition proceeded in vacuum chamber (background pressure $2'10^{-4}$ Pa) with constant rate ≈0.3 nm/s. Selected film was-deposited onto silicon single crystal wafer and subsequently annealed in inert Ar atmosphere at 90 ^{o}C for 2 hours.

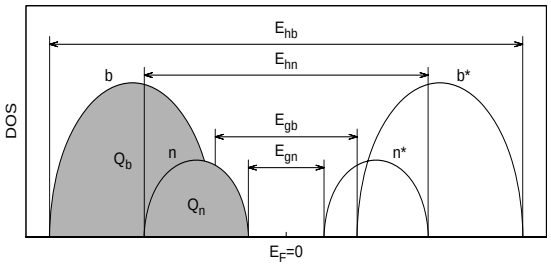

Fig. 2. Schema of the density of states corresponding to $As_{33}Se_{67}$ and as-deposited $Ge_2Sb_2Te_5$.

Our dispersion model of $As_{33}Se_{67}$ is based on the scheme of the electronic structure of valence and conduction bands presented in Fig. 2. A certain part of valence electrons is in bonding states. These valence states are split to bonding 'b' and anti-bonding 'b*' bands. A remaining part of the valence electrons that do not participate in the bond with neighbouring atoms form split non-bonding 'n' and anti-non-bonding 'n*' bands corresponding to the ground and excited state. The absorption of light is then caused by the transitions from valence to conduction bands, i. e. b→b* and n→n*. The cross transitions between bonding and non-bonding states, i. e. b→n* and n→b*, can be disregarded because the non-bonding electrons are partially localised, whereas the bonding electrons are in delocalised extended states and the probability of these transitions is small. Then the complex dielectric function is expressed as follows:

$$\hat{\varepsilon}(E) = 1 + \hat{\varepsilon}_{b \to b^*}(E) + \hat{\varepsilon}_{n \to n^*}(E) \tag{22}$$

where the contributions $\hat{}_{b®b^*}(E)$ and $\hat{}_{n®n^*}(E)$ are calculated using the PJDOS3 model. In this case the dispersion model contains the following six parameters: *Qb*, *Egb*, *Ehb*, *Qn*, *Egn* and *Ehn* (see Fig. 2).

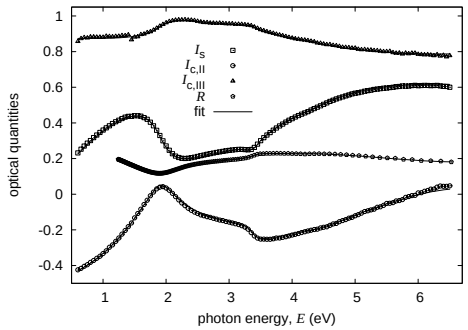

Fig. 3. Spectral dependencies of the optical quantities of the $As_{33}Se_{67}$ film: curves denote the theoretical data, points denote the experimental values.

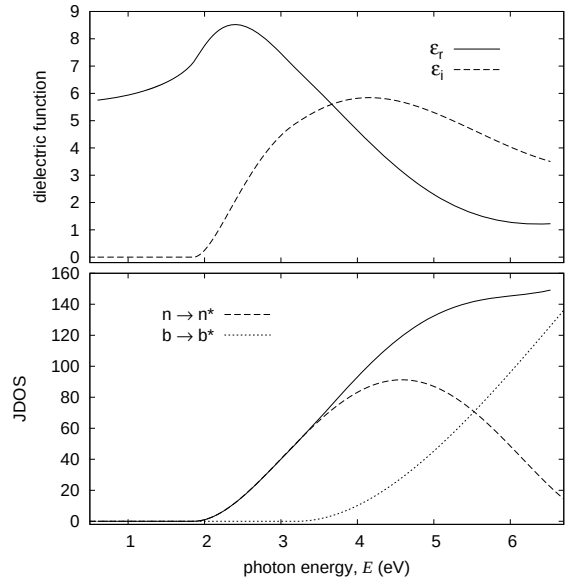

Fig. 4. Spectral dependencies of the real and imaginary part of the dielectric function (top) and JDOS (bottom) of the $As_{33}Se_{67}$ film.

Table 1. Dispersion parameters and thickness of the $As_{33}Se_{67}$ and GST films determined using the individual fits. Parameters fixed during the fitting are denoted with stars.

	$As_{33}Se_{67}$	as-deposited GST	annealed GST
Qn ($eV^{3/2}$)	16.3	17.1	18.7
Egn (eV)	1.852	0.803	0.587
Ehn (eV)	7.31	5.88	5.81
Cn	–	0.49	0.275
Gn	–	0.58	0.36
Hn	–	0*	-0.40
Qb ($eV^{3/2}$)	55.7	39.1	36.7
Egb (eV)	3.20	2.51	3.11
Ehb (eV)	20.7	14.2	14.9
Cb	–	0.5*	0.5*
Gb	–	0*	0.25
Hb	–	0*	0*
Qfc ($eV^{3/2}$)	–	–	3.5
Ew (eV)	–	–	4.1
$\bar{d}f$ (nm)	50.0	240	225
□	2.05	1.90	2.07

In Fig. 3 there are the spectral dependencies of the ellipsometric quantities and reflectances of the $As_{33}Se_{67}$ chalcogenide film. One can see that there is a very good agreement between the experimental and theoretical data. The theoretical curves were calculated using the parameter values found. In table 1 the values of the thickness and dispersion parameters determined for this sample are introduced. In Fig. 4 the spectral dependencies of both parts of the dielectric function calculated using the parameter values found are presented.

From the foregoing it follows that the PJDOS3 model is sufficient for interpretation of the experimental data corresponding to $As_{33}Se_{67}$. The efficiency of the combined method is also clear from the thickness value determined for this sample that is relatively small. Thus, this method is reliably applicable to the optical characterisation of relatively thin films in contrast to the optical methods based on measuring reflectance or transmittance. It is notable that this film exhibited non-negligible thickness non-uniformity that had to be included in the interpretation of the experimental data. The thickness value presented in table 1 represents the mean thickness of the film. The possibility to characterise the non-uniform thin films represents another advantage of the combined method.

5.2 $Ge_2Sb_2Te_5$ (GST)

The GST chalcogenide sample was-deposited onto the crystalline silicon wafer by pulsed laser deposition (PLD) technique [12, 28]. The sample was optically characterised as-deposited, then it was annealed at temperature of 180 ^{o}C and subsequently at temperature of 300 ^{o}C. After each annealing the sample was optically characterised. It should be noted that the complete optical characterisation performed earlier [12] utilised the PDOS model requiring the numerical integration in Eqs. (9) and (10). We perform the optical characterisation of the film using the same experimental data in the other way, i. e. we employ the analytical PJDOS model. For illustration the results corresponding to as-deposited and annealed at 300 ^{o}C samples are presented in this paper.

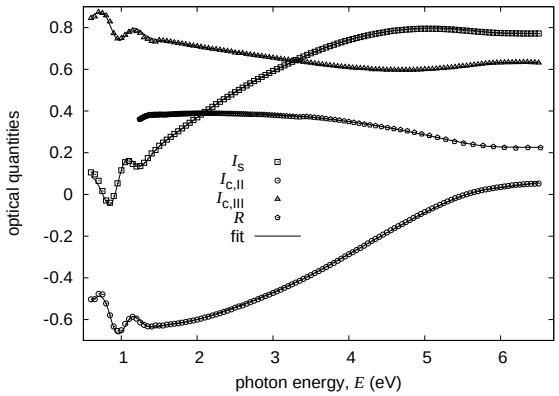

Fig. 5. Spectral dependencies of the optical quantities of the as-deposited $Ge_2Sb_2Te_5$ film: curves denote the theoretical data, points denote the experimental values.

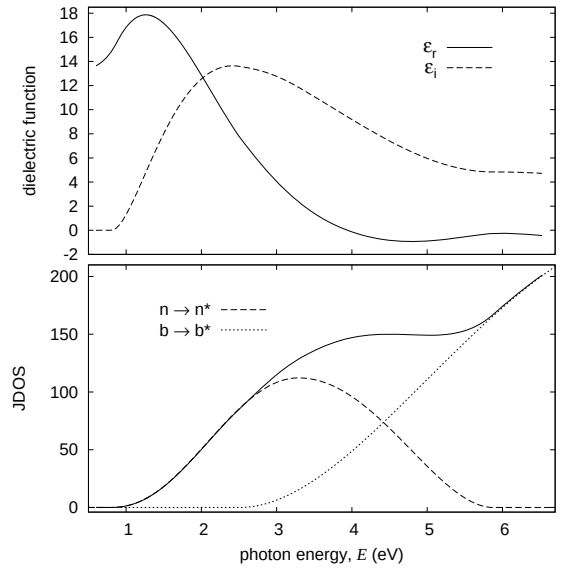

Fig. 6. Spectral dependencies of the real and imaginary part of the dielectric function (top) and JDOS (bottom) of the as-deposited $Ge_2Sb_2Te_2$ film.

First, we used the six parameter dispersion PJDOS3 model for characterising the as-deposited GST film. It was shown that this dispersion model was not sufficient for a satisfactory treatment of the experimental data. Therefore, we improved the fit by using the extended PJDOS6 dispersion model for expressing both the contributions in Eq. (22). The resulting dispersion model had the following twelve parameters: *Qb*, *Egb*, *Ehb*, *Cb*, *Gb*, *Hb*, *Qn*, *Egn*, *Ehn*, *Cn*, *Gn* and *Hn*. The results of the optical characterisation of the as-deposited GST film are summarised in Fig. 8 and 9 and table 1. Note that for the transitions between non-bonding states the full six parameter model was utilised, whereas, for the transitions between bonding states the parameters *Cb* and *Hb* were fixed because they do not influence the optical constants in the spectral region of interest. From Fig. 5 a good agreement between the experimental and theoretical data can be seen which supports the correctness of the results.

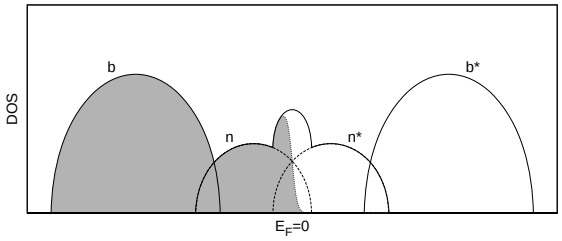

Fig. 7. Schema of the density of states corresponding to annealed $Ge_2Sb_2Te_5$.

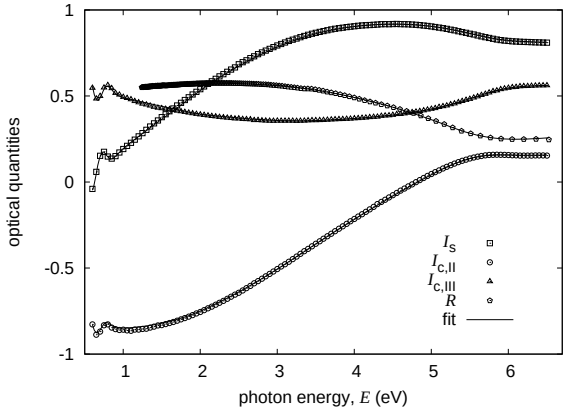

Fig. 8. Spectral dependencies of the optical quantities of the annealed $Ge_2Sb_2Te_5$ film: curves denote the theoretical data, points denote the experimental values.

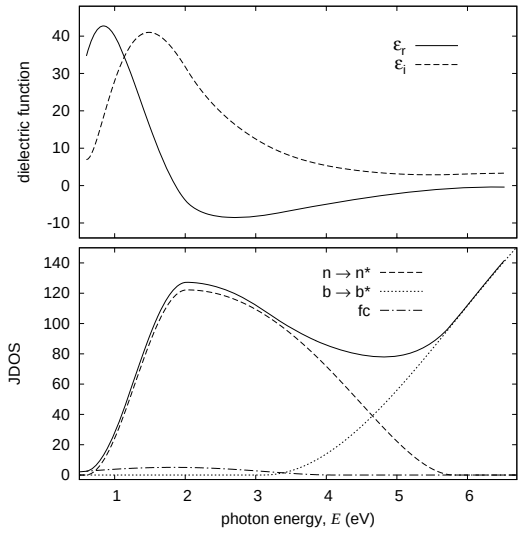

Fig. 9. Spectral dependencies of the real and imaginary part of the dielectric function (top) and JDOS (bottom) of the annealed $Ge_2Sb_2Te_5$ film.

It is known that annealed GST films are conductive. Therefore it was necessary to extend the dispersion model corresponding to the as-deposited film by the free carrier 'fc' contribution, i. e.

$$\hat{\varepsilon}(E) = 1 + \hat{\varepsilon}_{b\to b^*}(E) + \hat{\varepsilon}_{n\to n^*}(E) + \hat{\varepsilon}_{fc}(E) \qquad (23)$$

where the term, $\hat{\varepsilon}_{fc}(E)$ represents n→n and $n^*\to n^*$ intraband transitions in vicinity of the Fermi level. The existence of the free carrier contribution can be explained by overlapping the n and n^* bands corresponding non-bonding electrons after annealing (see Fig. 7).

The results of the optical characterisation of the GST film annealed at 300^{O}C are summarised in Fig. 8 and 9 and

Table 1. From the values of *Qb* and *Qn* it is clear that the number of bonding states decreased in consequence of the annealing while the number of non-bonding states increased. Moreover the corresponding energy gap *Egn* decreased and the contributions of free carriers appeared.

The total density of valence electrons, i. e. the sum of all *Q*, increased from value 56.2 for the as-deposited film to 58.9 for the annealed film (i. e. by 4.8%). This means that the film became denser. This is supported by the decreased of the film thickness from 240 to 225 nm (i. e. by 6.7%). However, the total number of valence electrons in the film could not change by heating unless desorption occurred during the annealing. The total number of valence electrons can be estimated as the product of the total *Q* and film thickness. The values of this product before and after annealing differ by 2.2%. It is not clear whether this difference is caused either by desorption of atoms or by experimental errors.

6. Conclusions

In this paper the optical characterisation of the $As_{33}Se_{67}$ and $Ge_2Sb_2Te_5$ chalcogenide thin films was carried out using the combined method of VASE and SR within the spectral region 0.6–6.5 eV. It was shown that this combined method is very useful and efficient for this purpose. This method enables us to determine both structural and dispersion parameters describing the thin films exhibiting various defects. The application of the combined method requires suitable structural and dispersion models of the film in order to fully utilise its advantages. Here, the structural models contained roughness, overlayers and thickness non-uniformity. The dispersion models employed were based on parametrisation of the JDOS. It was shown that the interband transitions could be described by either the three-parameter or six-parameter PJDOS model. The dielectric response of free carriers was also described by a two-parameter PJDOS model. The main advantage of the PJDOS models is that they, unlike the classical models based on Lorentz oscillator, are based on the assumption of finite bands which allows to introduce a parameter proportional to the density of electrons. It should be pointed out that using the method presented here it is possible to investigate quantitatively changes in the electronic structure of the materials caused by phase transitions which was demonstrated on GST. The method of the optical characterisation can be used to characterise other thin films exhibiting disordered structure.

Acknowledgements

This work was supported by Ministry of Education of the Czech Republic under the projects MSM 0021622411 and MSM 0021630518 and by the Czech Ministry of Trade under the project FT-TA3/142.

References

[1] E. Márquez, J. González-Leal, R. Prieto-Alcón, M. Vlček, A. Stronski, T. Wágner, D. Minkov, Appl. Phys. A **67**, 371 (1998).
[2] S. Yamanaka, S. Ogawa, I. Morimoto, Y. Ueshima, Jpn. J. Appl. Phys. **37,** 3327 (1998).
[3] I. Ohlídal, D. Franta, M. Frumar, J. Jedelský, K. Navrátil, J. Optoelectron. Adv. Mater. **3**, 873 (2001).
[4] D. Franta, I. Ohlídal, M. Frumar, J. Jedelský, Appl. Surf. Sci. **175-176**, 555 (2001).
[5] D. Franta, I. Ohlídal, M. Frumar, J. Jedelský, Appl. Surf. Sci. **212-213**, 116 (2003).
[6] I. Ohlídal, D. Franta, M. Frumar, J. Jedelský, J. Omasta, J. Optoelectron. Adv. Mater. **6**, 139 (2004).
[7] Y. Ruan, R. A. Jarvis, A. V. Rode, S. Madden, B. Luther-Davies, Opt. Commun. **252**, 39 (2005).
[8] B.-S. Lee, J. R. Abelson, S. G. Bishop, D.-H. Kang, B.-K. Cheong, K.-B. Kim, J. Appl. Phys. **97,** 093509 (2005).
[9] H. Dieker, M. Wutting, Thin Solid Films **478**, 248 (2005).
[10] E. Márquez, J. M. González-Leal, A. M. Bernal-Oliva, T. Wágner, R. Jiménez-Garay, J. Phys. D: Appl. Phys. **40**, 5351 (2007).
[11] A. Ganjoo, R. Golovchak, J. Optoelectron. Adv. Mater. **10**, 1328 (2008).
[12] D. Franta, M. Hrdlička, D. Nečas, M. Frumar, I. Ohlídal, M. Pavlišta, Phys. Status Solidi C **5**, 1324 (2008).
[13] D. Franta, D. Nečas, M. Frumar, Phys. Status Solidi C **6,** S59 (2009).
[14] S. O. Rice, Commun. Pure Appl. Math. **4**, 351 (1951).
[15] D. Franta, I. Ohlídal, J. Mod. Opt. **45**, 903 (1998).
[16] D. Franta, I. Ohlídal, Opt. Commun. **248**, 459 (2005).
[17] D. Franta, I. Ohlídal, J. Opt. A-Pure Appl. Opt**. 8**, 763 (2006).
[18] D. Franta, I. Ohlídal, D. Nečas, Opt. Express **16**, 7789 (2008).
[19] D. Nečas, I. Ohlídal, D. Franta, J. Opt. A-Pure Appl. Opt. **11,** 045202 (2009).
[20] I. Ohlídal, D. Franta, Ellipsometry of thin film systems, in: E. Wolf (Ed.), Progress in Optics **41**, Elsevier, Amsterdam, 181 (2000).
[21] N. F. Mott, E. A. Davis, Electronic Processes in Non-Crystalline Materials, Clarendon Press, Oxford, 1971.
[22] J. Tauc, Optical properties of non-crystaline solids, in: F. Abelès (Ed.), Optical Properties of Solids, North–Holland, Amsterdam, 277 (1972).
[23] S. Adachi, Optical Properties of Crystalline and Amorphous Semiconductors: Matrials and Fundamental Principles, Kluwer, Boston, 1999.
[24] P. Y. Yu, M. Cardona, Fundamentals of Semiconductors, Springer, Berlin, 2001.
[25] D. Franta, D. Nečas, L. Zajíčková, Opt. Express **15**, 16230 (2007).
[26] D. Franta, V. Buršíková, D. Nečas, L. Zajíčková, Diamond Relat. Mater. **17**, 705 (2008)
[27] R. de Laer Kronig, J. Opt. Soc. Am. & Rev. Sci. Instrum. **12**, 547 (1926).
[28] M. Frumar, B. Frumarová, P. Němec, T. Wágner, J. Jedelský, M. Hrdlička, J. Non-Cryst. Solids **352**, 544 (2006).

*Corresponding author: ohlidal@fme.vutbr.cz